Hydrophilic Hierarchical Nitrogen-Doped Carbon Nanocages for Ultrahigh Supercapacitive Performance

Jin Zhao, Hongwei Lai, Zhiyang Lyu, Yufei Jiang, Ke Xie, Xizhang Wang, Qiang Wu, Lijun Yang, Zhong Jin, Yanwen Ma, Jie Liu, and Zheng Hu**

Supercapacitors feature high power density and long cycle life, and present increasing significance as the advanced energy storage devices. They are classified into electrical double layer capacitors (EDLCs) and pseudocapacitors according to the different capacitive mechanisms.[1] EDLCs store the charges in electrical double layer by the electrostatic adsorption of electrolyte ions onto the charged surface of electrodes, whereas pseudocapacitors store energy through Faradaic redox reaction. EDLCs possess higher power density and longer cycling stability, but lower energy density than pseudocapacitors.[1,2] The energy density (E) of a supercapacitor is described as

$$E = \frac{1}{2}CV^2 \quad (1)$$

where C is the capacitance and V the operation voltage. To increase the energy density, usually there are two approaches, i.e., increasing C or/and V. As known, the supercapacitive performance of an EDLC electrode material is closely associated with the specific surface area as well as the transport kinetics of electrons and ions. In general, an ideal EDLC electrode material should feature: (i) the high specific surface area to ensure the space for charge storage, (ii) the well-balanced pore distribution to improve both specific capacitance and rate capability, (iii) the high conductivity to ensure high rate capability and power density, and (iv) the good wettability to facilitate ion diffusion and increase ion-accessible surface area.[1,2]

Carbon materials of sp^2 hybridization usually have good conductivity, abundant structures and morphologies, thus are the main option to explore the advanced EDLC electrode materials.[2a–c] Various carbon materials such as activated carbon (AC),[3] carbon nanotubes (CNTs),[4] and graphene[5] have been intensively studied, which demonstrate different features as briefly summarized in our recent paper.[6] Regarding the performance, the graphene-based material seems to be the most promising one due to the high conductivity, high theoretical specific surface area (2630 $m^2\ g^{-1}$), and specific capacitance (550 $F\ g^{-1}$).[7] However, the strong π–π interaction between graphene sheets would cause inevitable aggregation and restacking, which loses the high specific surface area of individual graphene sheets and deteriorates the specific capacitance. Hence, complex treatments are usually needed, e.g., by designing 3D graphene,[8] introducing spacer between graphene sheets,[9] and creating crumples[10] or pores[11] on the sheets. By in situ MgO template method, we recently obtained the carbon nanocages (CNCs) with large specific surface area and regular framework, which demonstrate a large specific capacitance, high rate capability, and excellent stability in aqueous electrolytes, comparable to the state-of-the-art EDLC electrode materials.[6] Despite the good supercapacitive performance of CNCs, the areal capacitance normalized by specific surface area, i.e., the area-normalized capacitance, is still at the ordinary level of carbon materials, about ≈11.7 $\mu F\ cm^{-2}$ at the current density of 1 $A\ g^{-1}$. This means there is still plenty room to further improve the supercapacitive performance with this new carbon architecture. As known, normally the pure carbon material is hydrophobic, preventing water from getting into small pores, thus limits the effective surface area of the material. Hence, a possible solution to maximize the supercapacitive potential of CNCs in aqueous electrolyte is to improve its wettability toward water while without sacrificing other outstanding properties, by referring to the aforementioned prerequisites for an ideal EDLC electrode material. In our recent studies, we found that, doping sp^2 carbon with heteroatoms such as B and N could effectively modulate the electronic structure and oxygen reduction performance.[12] This approach should also be the best choice to increase the CNCs' wettability since it does not change the morphological merits of the materials. In this study, hierarchical nitrogen-doped carbon nanocages (hNCNCs) were prepared by in situ MgO template method and the products feature a large specific surface area, multiscale porous structure, and much improved wettability. All the hNCNCs deliver the higher area-normalized capacitances than the corresponding hierarchical carbon nanocages (hCNCs) prepared at the same temperature. Especially, the hNCNC prepared at 800 °C exhibits an ultrahigh specific capacitance up to 313 $F\ g^{-1}$ at 1 $A\ g^{-1}$ (17.4 $\mu F\ cm^{-2}$) with excellent rate capability and cycling stability. Together with

J. Zhao, H. Lai, Z. Lyu, Y. Jiang, K. Xie, Prof. X. Wang, Prof. Q. Wu, Dr. L. Yang, Prof. Z. Jin, Prof. Z. Hu
Key Laboratory of Mesoscopic Chemistry of MOE and Collaborative Innovation Center of Chemistry for Life Sciences
Jiangsu Provincial Lab for Nanotechnology
School of Chemistry and Chemical Engineering
Nanjing University
Nanjing 210093, China
E-mail: wangxzh@nju.edu.cn; zhenghu@nju.edu.cn
Prof. Y. Ma
Jiangsu Key Lab for Organic Electronics and Information Displays & Institute of Advanced Materials
Nanjing University of Posts and Telecommunications
Nanjing 210046, China
Prof. J. Liu
Department of Chemistry
Duke University
Durham, NC 27708, USA

DOI: 10.1002/adma.201500945

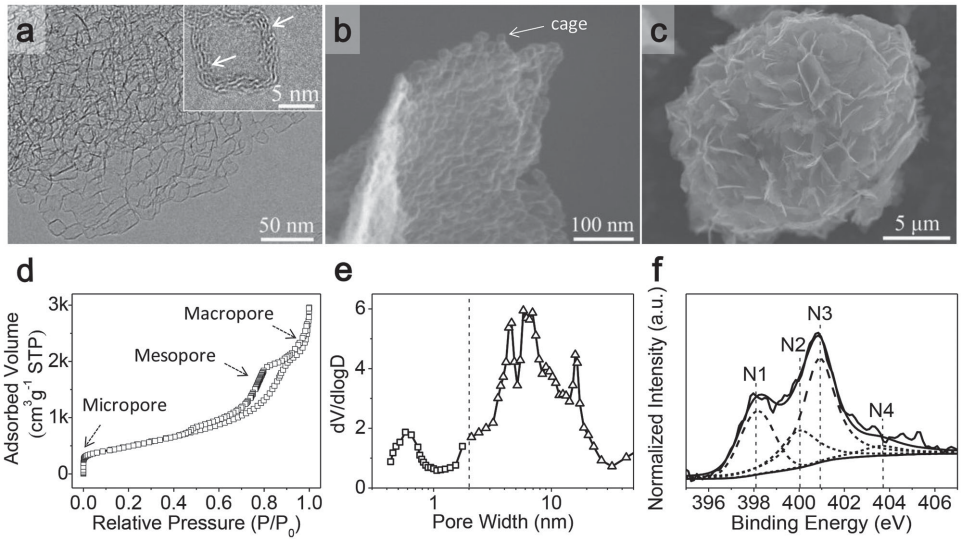

Figure 1. Morphological and structural characterizations of the hNCNC800. a) TEM image. Inset is the corresponding high-resolution TEM image. Arrows indicate the broken fringes. b,c) SEM images of different magnifications. d) Nitrogen adsorption and desorption isotherm. e) Size distributions of the micropores and mesopores. The dashed line marks the boundary. The existence of macropores is reflected by the steep uptake at $P/P_0 > 0.97$ in (d)[13]. f) N1s XPS spectrum. Note: N1, N2, N3, N4 denote pyridinic, pyrrolic, graphitic nitrogen, and pyridine-*N*-oxide group, respectively.

the convenient preparation and low cost, the hNCNCs provide us a new kind of top-ranking EDLC electrode materials with great potential applications.

The hNCNCs synthesized at 700, 800, and 900 °C were designated as hNCNC700, hNCNC800, and hNCNC900, respectively. For comparison, the corresponding hCNCs were also prepared with similar conditions, designated as hCNC700, hCNC800, and hCNC900 (see the Experimental Section).

Figure 1 shows the typical morphological and structural characterizations of the hNCNC800. The building blocks are the cuboidal hollow nanocages of ≈10–25 nm in size and ≈5 graphitized layers in thickness as learnt from the transmission electron microscopy (TEM) image (Figure 1a). It is noteworthy that these nanocages interconnect to form the micrometer-sized nanosheets, which further assemble into the 3D sphere-like particles of 10–30 μm in sizes with a large intersheet space as shown in the scanning electron microscopy (SEM) images (Figure 1b,c). N_2 adsorption/desorption isotherm exhibits a typical IV-type curve with two steep uptakes ($P/P_0 < 0.01$, $P/P_0 > 0.97$) and a hysteresis loop ($0.40 < P/P_0 < 0.90$), indicating the coexistence of micropores (<2 nm), mesopores (2–50 nm), and macropores (>50 nm) (Figure 1d,e). The micropores distribute around ≈0.6 nm in size, in accordance with the observed broken fringes in the graphitized shells (inset in Figure 1a), which can serve as the tunnels for ion transfer between the inside and outside of the nanocages.[13] Such unique multiscale porous structure is beneficial to achieving the high specific surface area and fast charge (ion and electron) transfer which is favorable for most electrochemical processes.[13] Other five samples exhibit the similar morphological and structural features (Figure S1, Supporting Information). The 3D configuration and multiscale porous structure endows the hNCNC700, hNCNC800, and hNCNC900 with high specific surface areas of 2407, 1794, and 1529 $m^2 g^{-1}$, respectively. The corresponding N contents of 10.6, 7.9, and 6.8 at% are obtained by X-ray photoelectron spectroscopy (XPS) analysis. Thermogravimetry (TG) monitoring of the oxidation indicates the effective removal of MgO template, and the increasing crystallinity with increasing growth temperature (Figures S2–S4, Supporting Information).

The above characterization results indicate the unique hNCNCs are obtained with the features of multiscale porous structure and high specific surface area. To learn the effect of N-doping on wettability, the dynamic water contact angle measurements were performed for the samples as illustrated in **Figure 2**. Quite different wetting processes were observed for the hNCNCs and hCNCs. The hCNC800 is very hydrophobic

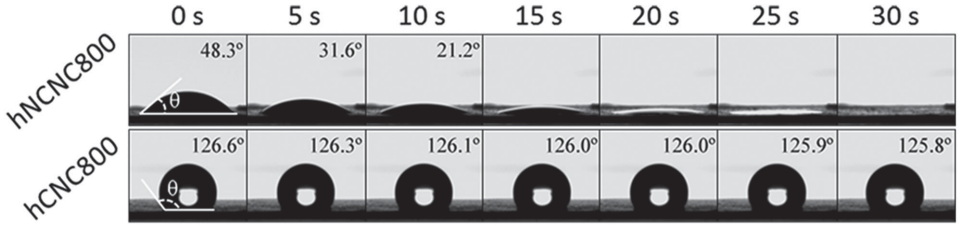

Figure 2. Dynamic water contact angle measurement for the hNCNC800 and hCNC800. The photograph at 0 s was taken immediately after resting the water droplet on the surface.

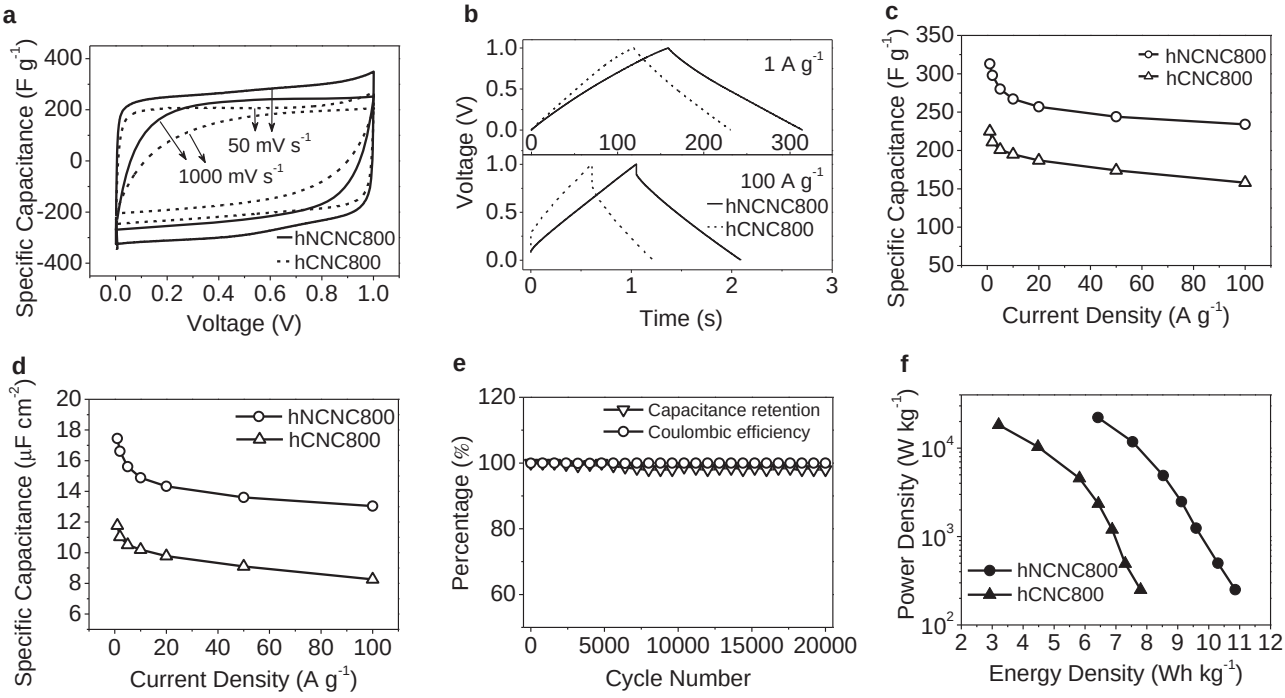

Figure 3. Electrochemical characterizations of the hNCNC800-SC and hCNC800-SC in 6 M KOH electrolyte. a) CV curves at the scan rates of 50 and 1000 mV s^{-1}. b) CP curves at the current densities of 1 and 100 A g^{-1}. c) Gravimetric capacitances at different charge–discharge current densities. d) Area-normalized capacitances at different charge–discharge current densities. e) Cycling stability and Coulombic efficiency of the hNCNC800-SC at 10 A g^{-1}. f) Ragone plots.

with the initial contact angle of 126.6°, which remains almost unchanged for 30 s or the longer. In contrast, the hNCNC800 is very hydrophilic with the initial contact angle of 48.3° and the droplet is completely absorbed within 20 s. This result clearly indicates the much improved wettability of the hNCNCs over the hCNCs due to the introduced polar C–N bonds by nitrogen doping as expected,[14] which favors the exploration of the advanced EDLC electrode materials (Figure S5, Supporting Information).

To evaluate the supercapacitive performance of the hNCNCs, two-electrode coin-type supercapacitors were fabricated with 6 mol L^{-1} KOH aqueous solution as electrolyte. **Figure 3** shows the typical electrochemical performances for the hNCNC800- and hCNC800-based supercapacitors, denoted as hNCNC800-SC and hCNC800-SC, respectively. Both cyclic voltammetry (CV) curves show nearly symmetrical rectangular shapes at the scan rate of 50 mV s^{-1}. With increasing the scan rate to 1000 mV s^{-1}, the hNCNC800-SC still keeps a rather good rectangular-like CV curve, much better than the case for the hCNC800-SC (Figure 3a). The different evolutions clearly indicate the better supercapacitive behavior and rate capability, as well as the smaller equivalent series resistance (ESR) for the hNCNC800-SC than the hCNC800-SC (Figure S6, Supporting Information).[6,8a-c] The chronopotentiometry (CP) curves of the hNCNC800-SC show highly symmetry and nearly linear slopes even at the high current density of 100 A g^{-1} with a rather limited voltage (*IR*) drop, which gives an ultrahigh gravimetric capacitance of 313 F g^{-1} at 1 A g^{-1} and 234 F g^{-1} at 100 A g^{-1} (≈75% retention) for the hNCNC800 electrode (Figure 3b,c). For all the tested current densities in the range of 1–100 A g^{-1}, the hNCNC800-SC exhibits the smaller *IR* drop with the slower increasing tendency than the hCNC800-SC, in consistent with the smaller ESR for the former as learnt from the CV evaluation (Figures S7 and S8, Supporting Information). Moreover, the hNCNC800 presents the obvious higher gravimetric capacitance than the hCNC800 although the specific surface area is smaller for the former (1794 m^2 g^{-1}) than the latter (1912 m^2 g^{-1}) (Figure 3c). As a result, the area-normalized capacitance of the hNCNC800 is much higher than that of the hCNC800, e.g., 17.4 versus 11.8 μF cm^{-2} at 1 A g^{-1} (Figure 3d and Figure S9, Supporting Information). In addition, the hNCNC800-SC displays a high stability of ≈98% capacitance retention after 20 000 cycles at the high current density of 10 A g^{-1} with the Coulombic efficiency of ≈100% through the testing cycles (Figure 3e and Figure S10, Supporting Information). Actually, all the six samples in this study demonstrate the high-level supercapacitive performance,[2c,3b,8b] and the optimal hNCNC800 presents the better performance than the most carbon-based materials to date with comparable test condition (Table S1, Supporting Information). Ragone plots further demonstrate the best performance of the hNCNC800-SC among the six supercapacitors, which stays at the state-of-the-art level for the carbon-based supercapacitors in aqueous electrolyte (Figure 3f and Figure S11, Supporting Information).[15] The energy density of the hNCNC800-SC reaches 10.90 and 6.42 Wh kg^{-1} with the corresponding average power density of 0.25 and 22.22 kW kg^{-1} at 1 and 100 A g^{-1}, respectively. The high-level supercapacitive performances of the hNCNCs and hCNCs mainly result from the unique 3D porous hierarchical structure which combines the advantages of high specific surface area, suitable pore

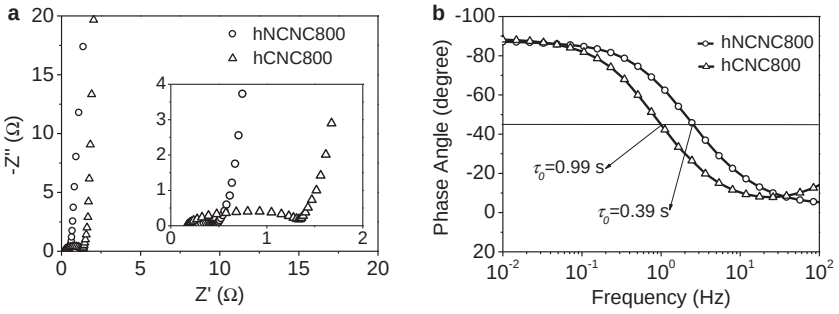

Figure 4. Frequency responses of the hNCNC800-SC and hCNC800-SC in 6 M KOH electrolyte. a) Nyquist plots. Inset magnifies the high-frequency range. b) Bode plots of phase angle versus frequency.

structure, and good conductivity. The synergism of these characteristics ensures the sufficient space for charge storage and the fast transport for ions and electrons, therefore demonstrating the large specific capacitance, high rate capability, and excellent cycling stability (Table S1, Supporting Information). In comparison with the hCNCs, the hNCNCs possess the much better wettability due to N-doping which further increases the ion-accessible surface area and facilitates the ion diffusion. Hence, the optimal hNCNC800-SC shows the best performance.

To further ascertain the effect of wettability, the electrochemical impedance spectroscopy was performed as shown in **Figure 4** (Figure S12, Supporting Information). In the Nyquist plot, the intrinsic ohmic resistance (the first intercept along the real axis) of the hNCNC800-SC is slightly larger than that of the hCNC800-SC (Figure 4a), as supported by the conductivity measurements (Figure S13, Supporting Information). The vertical curve in the low-frequency region indicates the nearly ideal capacitive behavior.[8a–c,16] By extrapolating the vertical portion to the real axis, the ESR of 0.56 and 1.64 Ω is obtained for the hNCNC800-SC and hCNC800-SC, respectively. The difference of 1.08 Ω for the two ESR values mainly results from the smaller charge transfer resistance (the diameter of the semicircle) of the hNCNC800-SC (0.23 Ω) than the hCNC800-SC (1.32 Ω), with 1.09 Ω difference (inset in Figure 4a). The much smaller charge transfer resistance for the hNCNC800-SC than the hCNC800-SC originates from the larger ion-accessible surface area and the faster ion diffusion due to the much better wettability for the former (Figure 2).[9a,17] Hence, though the hNCNC800-SC has the slightly larger intrinsic ohmic resistance than the hCNC800-SC (Figure 4a), the ESR of the former is still much smaller than the latter, leading to the smaller *IR* drop (Figure 3b). The phase angles are close to -90° at the low-frequency region in the Bode plots, which also indicates the ideal capacitive behavior of the two supercapacitors (Figure 4b).[7,16] The characteristic frequency f_0 at the phase angle of –45° is 2.58 Hz for the hNCNC800-SC and 1.01 Hz for the hCNC800-SC, corresponding to the time constant τ_0 ($\tau_0 = 1/f_0$) of 0.39 and 0.99 s, respectively. The much shorter time constant for the hNCNC800-SC than the hCNC800-SC indicates the faster charge–discharge rate and the higher power density for the former thereof.[7,16]

As known, to increase the energy density of the EDLCs, ionic liquids or organic solvents are often employed as electrolytes due to their high operating voltage. In these cases, similar strategy should be still valid, i.e., to increase the wettability between the hCNCs and the electrolytes by means of suitable doping or surface modification.

In summary, we have obtained the unique 3D hierarchical nitrogen-doped carbon nanocages, which integrate the advantages of large specific surface area, multiscale porous structure, good conductivity, and excellent wettability. The synergism of these characteristics ensures the sufficient space for charge storage and the fast transport for ions and electrons. The optimal hNCNC800 exhibits a large area-normalized capacitance of 17.4 μF cm^{-2} and an ultrahigh specific capacitance up to 313 F g^{-1} at 1 A g^{-1}. The corresponding supercapacitor delivers the high energy density (10.90 Wh kg^{-1}) and power density (22.22 kW kg^{-1}), as well as excellent rate capability and cycling stability. The state-of-the-art supercapacitive performance of the hNCNCs is even much better than the high-level performance for the undoped hCNCs. Such a step forward is attributed to the greatly improved hydrophilicity due to N-doping which effectively increases the ion-accessible surface, facilitates the ion diffusion, thus reduces the charge transfer resistance and ESR of the device. Together with the convenient preparation and low cost, the 3D hierarchical nitrogen-doped carbon nanocages provide us a new kind of top-ranking EDLC electrode materials with great potential applications.

Experimental Section

Preparation of hNCNC and hCNC: The samples were prepared by the convenient in situ MgO template method as described in our recent paper,[13] with a little of modification. In a typical procedure, basic magnesium carbonate ($4MgCO_3{\cdot}Mg(OH)_2{\cdot}5H_2O$) (4 g) with 3D hierarchical structure was placed into a quartz tube in a vertical furnace. For the growth of hNCNC800, the furnace was heated up to 800 °C in Ar at the flow rate of 100 sccm and heating rate of 10 °C min^{-1}. Then pyridine was introduced into the tube at the feeding rate of 65 μL min^{-1} by a syringe pump for 4 min. During the growth, the sample was remixed by a flash of high-rate Ar flow of 1200 sccm with the interval of 1 min. The reactor was thus naturally cooled down to room temperature. The as-prepared sample was first stirred in 6 M HCl aqueous solution for 48 h to remove the MgO template and repeatedly washed with deionized water. Finally, the hNCNC800 (≈180 mg) was obtained after drying at 80 °C for 24 h. Similarly, the hNCNC700, hNCNC900, hCNC700, hCNC800, and hCNC900 were obtained. Benzene was used as the precursor for the preparation of hCNC.

Structural Characterizations: SEM (Hitachi S4800 at 10 kV), TEM (JEM-2100F operating at 200 kV), and XPS (PHI 5000 VersaProbe) were used for the characterizations of morphologies, structures, and components of the products. N_2 adsorption/desorption isotherms were measured on Thermo Fisher Scientific Surfer Gas Adsorption Porosimeter at 77 K. Before measurement, the sample was degassed at 300 °C for 6 h. The specific surface area was calculated using the Brunauer–Emmett–Teller (BET) method based on the adsorption data in the linear relative pressure (P/P_0) range of 0.05–0.30. The pore size distribution was calculated from the corresponding adsorption branch of N_2 isotherm by Horvath–Kawazoe method for micropore and Barrett–Joyner–Halenda method for mesopore. Thermogravimetry analysis (Netzsch STA-449F3) was performed at a heating rate of 10 °C min^{-1} under 20% O_2/Ar. The conductivity was measured by a four-wire method using a source measure unit (Keithley 6430, Figure S13, Supporting Information).

Dynamic Water Contact Angle Measurements: The powder sample was first wetted with ethanol and then rolled into sheet on aluminum foil. After dried at 80 °C for 12 h, the evolution of the water contact angle was recorded by the contact angle measurement system (OCA 30, DataPhysics Instruments GmbH).

Fabrication of Supercapacitors: Symmetric supercapacitor of coin-cell type was fabricated to evaluate the supercapacitive performance of the products. Briefly, 80 wt% product, 15 wt% conducting carbon, and 5 wt% PTFE (60 wt% dispersion in water) were homogeneously mixed into a paste using an agate mortar and pestle. Then the mixture was rolled on to the current collector of nickel foam with a diameter of 1.4 cm. After dried at 120 °C for 6 h, the electrodes/collectors were assembled in CR2032 stainless steel coin cell with the porous cellulose membrane and 6 M KOH aqueous solution as separator and electrolyte, respectively. The active material on each electrode was 1.0 mg. The thickness of the electrode film is estimated to be about 30 μm by SEM, which is larger than the recommended value of 15 μm for commercial supercapacitors (Figure S14, Supporting Information).[18]

Electrochemical Characterizations and Calculations: VMP3 Electrochemical Workstation (Bio-logic) was used for electrochemical evaluation. The electrochemical impedance spectroscopy was performed at open circuit potential with a sinusoidal signal over a frequency range from 100 kHz to 10 mHz at an amplitude of 10 mV. The cycling test was evaluated by chronopotentiometry charge/discharge measurement.

Specific capacitance of the electrode material (C_s, F g^{-1}) was calculated from CP discharge curve

$$C_s = \frac{2 \times I_{cons} \times \Delta t}{m \times \Delta V} \quad (2)$$

where I_{cons} is the constant current in discharging, m the mass of active material on one electrode, Δt the discharge time, and ΔV the voltage change during discharge (excluding the *IR* drop).

Energy density (E, Wh kg^{-1}) of the cell was calculated by

$$E = \frac{C_s \times V_{max^2}}{2 \times 4 \times 3.6} \quad 3)$$

where V_{max} is the voltage at the beginning of discharge.

Note: With the factor 4, the specific capacitance of electrode material (C_s) is converted to the capacitance of the cell based on the total mass of active material. With the factor 3.6, the unit of energy density (E) is converted from J g^{-1} to Wh kg^{-1}.

Average power density (P, W kg^{-1}) of the cell was obtained by

$$P = \frac{E \times 3600}{\Delta t} \quad (4)$$

Supporting Information

Supporting Information is available from the Wiley Online Library or from the author.

Acknowledgements

This work was jointly supported by NSFC (51232003, 21373108, 21473089, 21203092, 21173115), "973" program (2013CB932902), Suzhou Program (ZXG2013025), and the Priority Academic Program Development of Jiangsu Higher Education Institutions.

Received: February 24, 2015
Revised: March 30, 2015
Published online: April 30, 2015

[1] a) B. E. Conway, *Electrochemical Supercapacitors: Scientific Fundamentals and Technological Applications*, Kluwer, New York **1999**; b) G. Wang, L. Zhang, J. Zhang, *Chem. Soc. Rev.* **2012**, *41*, 797; c) P. Simon, Y. Gogotsi, B. Dunn, *Science* **2014**, *343*, 1210; d) X. Lu, M. Yu, G. Wang, Y. Tong, Y. Li, *Energy Environ. Sci.* **2014**, *7*, 2160.

[2] a) Y. Zhai, Y. Dou, D. Zhao, P. F. Fulvio, R. T. Mayes, S. Dai, *Adv. Mater.* **2011**, *23*, 4828; b) C. Liu, F. Li, L. P. Ma, H. M. Cheng, *Adv. Mater.* **2010**, *22*, E28; c) J. Yan, Q. Wang, T. Wei, Z. Fan, *Adv. Energy Mater.* **2014**, *4*, 1300816; d) X. Peng, L. Peng, C. Wu, Y. Xie, *Chem. Soc. Rev.* **2014**, *43*, 3303.

[3] a) L. Wei, G. Yushin, *Nano Energy* **2012**, *1*, 552; b) M. Sevilla, R. Mokaya, *Energy Environ. Sci.* **2014**, *7*, 1250.

[4] Z. Cao, B. Q. Wei, *Energy Environ. Sci.* **2013**, *6*, 3183.

[5] a) L. L. Zhang, R. Zhou, X. S. Zhao, *J. Mater. Chem.* **2010**, *20*, 5983; b) Y. Huang, J. Liang, Y. Chen, *Small* **2012**, *8*, 1805; c) X. Cao, Z. Yin, H. Zhang, *Energy Environ. Sci.* **2014**, *7*, 1850.

[6] K. Xie, X. Qin, X. Wang, Y. Wang, H. Tao, Q. Wu, L. Yang, Z. Hu, *Adv. Mater.* **2012**, *24*, 347.

[7] a) Z. Wu, K. Parvez, X. Feng, K. Müllen, *Nat. Commun.* **2013**, *4*, 2487; b) M. F. El-Kady, V. Strong, S. Dubin, R. B. Kaner, *Science* **2012**, *335*, 1326.

[8] a) L. Zhang, G. Shi, *J. Phys. Chem. C* **2011**, *115*, 17206; b) Y. Li, Z. Li, P. K. Shen, *Adv. Mater.* **2013**, *25*, 2474; c) U. N. Maiti, J. Lim, K. E. Lee, W. J. Lee, S. O. Kim, *Adv. Mater.* **2014**, *26*, 615; d) X. Xia, D. Chao, Z. Fan, C. Guan, X. Cao, H. Zhang, H. J. Fan, *Nano Lett.* **2014**, *14*, 1651.

[9] a) X. Yang, C. Cheng, Y. Wang, L. Qiu, D. Li, *Science* **2013**, *341*, 534; b) Z. Fan, J. Yan, L. Zhi, Q. Zhang, T. Wei, J. Feng, M. Zhang, W. Qian, F. Wei, *Adv. Mater.* **2010**, *22*, 3723; c) N. Jung, S. Kwon, D. Lee, D. M. Yoon, Y. M. Park, A. Benayad, J. Y. Choi, J. S. Park, *Adv. Mater.* **2013**, *25*, 6854.

[10] a) Z. Wen, X. Wang, S. Mao, Z. Bo, H. Kim, S. Cui, G. Lu, X. Feng, J. Chen, *Adv. Mater.* **2012**, *24*, 5610; b) Y. Yoon, K. Lee, C. Baik, H. Yoo, M. Min, Y. Park, S. M. Lee, H. Lee, *Adv. Mater.* **2013**, *25*, 4437.

[11] a) Y. Zhu, S. Murali, M. D. Stoller, K. J. Ganesh, W. Cai, P. J. Ferreira, A. Pirkle, R. M. Wallace, K. A. Cychosz, M. Thommes, D. Su, E. A. Stach, R. S. Ruoff, *Science* **2011**, *332*, 1537; b) X. Han, M. R Funk, F. Shen, Y. C. Chen, Y. Li, C. J. Campbell, J. Dai, X. Yang, J. W. Kim, Y. Liao, J. W. Connell, V. Barone, Z. Chen, Y. Lin, L. Hu, *ACS Nano* **2014**, *8*, 8255.

[12] a) L. Yang, S. Jiang, Y. Zhao, L. Zhu, S. Chen, X. Wang, Q. Wu, J. Ma, Y. Ma, Z. Hu, *Angew. Chem. Int. Ed.* **2011**, *50*, 7132; b) S. Chen, J. Bi, Y. Zhao, L. Yang, C. Zhang, Y. Ma, Q. Wu, X. Wang, Z. Hu, *Adv. Mater.* **2012**, *24*, 5593; c) Y. Zhao, L. Yang, S. Chen, X. Wang, Y. Ma, Q. Wu, Y. Jiang, W. Qian, Z. Hu, *J. Am. Chem. Soc.* **2013**, *135*, 1201; d) H. Feng, J. Ma, Z. Hu, *J. Mater. Chem.* **2010**, *20*, 1702.

[13] Z. Lyu, D. Xu, L. Yang, R. Che, R. Feng, J. Zhao, Y. Li, Q. Wu, X. Wang, Z. Hu, *Nano Energy* **2015**, *12*, 657.

[14] a) Z. Y. Jin, A. H. Lu, Y. Y. Xu, J. T. Zhang, W. C. Li, *Adv. Mater.* **2014**, *26*, 3700; b) W. J. Lee, U. N. Maiti, J. M. Lee, J. Lim, T. H. Han, S. O. Kim, *Chem. Commun.* **2014**, *50*, 6818.

[15] a) L. F. Chen, X. D. Zhang, H. W. Liang, M. Kong, Q. F. Guan, P. Chen, Z. Y. Wu, S. H. Yu, *ACS Nano* **2012**, *6*, 7092; b) Y. Tan, C. Xu, G. Chen, Z. Liu, M. Ma, Q. Xie, N. Zheng, S. Yao, *ACS Appl. Mater. Interfaces* **2013**, *5*, 2241; c) X. Wang, Y. Zhang, C. Zhi, X. Wang, D. Tang, Y. Xu, Q. Weng, X. Jiang, M. Mitome, D. Golberg, Y. Bando, *Nat. Commun.* **2013**, *4*, 2905; d) L. F. Chen, Z. H. Huang, H. W. Liang, H. L. Gao, S. H. Yu, *Adv. Funct. Mater.* **2014**, *24*, 5104.

[16] a) Z. Bo, W. Zhu, W. Ma, Z. Wen, X. Shuai, J. Chen, J. Yan, Z. Wang, K. Cen, X. Feng, *Adv. Mater.* **2013**, *25*, 5799; b) Y. Xu, Z. Lin, X. Zhong, X. Huang, N. O. Weiss, Y. Huang, X. Duan, *Nat. Commun.* **2014**, *5*, 4554; c) Y. Yoon, K. Lee, S. Kwon, S. Seo, H. Yoo, S. Kim, Y. Shin, Y. Park, D. Kim, J. Y. Choi, H. Lee, *ACS Nano* **2014**, *8*, 4580.

[17] a) X. Li, J. Rong, B. Q. Wei, *ACS Nano* **2010**, *4*, 6039; b) J. Luo, H. D. Jang, J. Huang, *ACS Nano* **2013**, *7*, 1464.

[18] M. D. Stoller, R. S. Ruoff, *Energy Environ. Sci.* **2010**, *3*, 1294.